

# Flow around a flexible plate in a free stream<sup>†</sup>

JiSeok Lee and SangHwan Lee<sup>\*</sup>

*Department of Mechanical Engineering, Hanyang University, 17 Haengdang-dong, Seongdong-gu, Seoul, 133-791, Korea*

(Manuscript Received May 28, 2010; Revised September 10, 2010; Accepted October 4, 2010)

## Abstract

This paper presents a numerical scheme for fluid-structure interaction, especially for flexible structures. The lattice Boltzmann method with an immersed boundary technique using a direct forcing scheme is used for the fluid, and a finite element method with Euler beam elements is used for the flexible plate. The direct forcing scheme of the lattice Boltzmann method was improved for the immersed boundary scheme by introducing the occupation ratio of fluid lattices among the interpolated lattices. We compared the results of our proposed scheme with the known results of conventional schemes. Using the proposed numerical scheme, the flow around the flexible plate in a free stream is simulated for the effect of flexibility. Our results show that the major role of the flexibility of the flexible plate is the reduction of the resistance from flow. From the unsteady flow around a flexible plate, we found that the  $St$  of the flexible plate up to  $Re < 80$  increased regardless of plate flexibility, but the  $St$  in the range of  $Re > 120$  was dependent on plate flexibility. In the range of  $Re > 120$ , the  $St$  of very flexible plate increased with increasing  $Re$ , while the  $St$  of rigid plate decreased with increasing  $Re$ .

*Keywords:* Boltzmann method; Flexible plate; Finite element method; Fluid-structure interaction

## 1. Introduction

Fluid-structure interaction problems are important in many areas, such as fish locomotion, insect flight, wind turbine blade and flow-induced vibration of pressurized water reactors in nuclear power. Many issues must be resolved to achieve accurate and efficient simulation of fluid-structure interaction. The treatments of the moving fluid-solid interface are critical for fluid solvers, noise reduction induced by flow for the solid solver and the coupling of both solvers in the time domain. Fluid solvers based on Navier-Stokes equations are commonly used. There are a variety of methods to solve the Navier-Stokes equations in the fluid domain with moving boundaries. These methods can be classified into two categories, depending on whether a moving mesh or fixed mesh is used. The arbitrary Lagrange-Eulerian method (ALE) [1–4] is a moving mesh type solver that reconstructs the mesh with the motion of the structure. It has high-order accuracy but can be computationally intensive according to the complexity of boundary shape and motion. If the structure undergoes large deformations, the re-meshing procedure will be very difficult. The distributed-Lagrange-multiplier/fictitious-domain method (DLM/FD) [5, 6] is a fixed mesh type solver. Fixed mesh methods are simple and efficient

because the solver does not require re-meshing, but they have limits in describing the boundaries accurately because the grid is non-adaptive.

Since the 1990's the lattice Boltzmann method (LBM) has been widely used for fluid solver instead of solving the Navier-Stokes equations [7, 8]. The LBM is basically a fixed mesh type solver. Numerous schemes are being published and developed for moving boundaries with accuracy. Bouzidi et al. [9] used well-organized interpolation for the unknown distribution of a curved boundary with precise second-order accuracy and proposed a scheme for a general moving boundary. Lallemand and Luo [10] developed the interpolated bounce back scheme with second order accuracy and applied it to a moving cylinder in a channel. If the boundaries are complex and moving, the scheme using interpolation or extrapolation has the possibility of a lack of information for interpolation. Lee and Lee [11] improved the accuracy without additional neighbor lattice information using the adaptive relaxation time. Feng and Michaelides [12, 13] adopted the immersed boundary method with direct forcing method to the LBM to simulate particulate flows including collisions. Sui et al. [14] reported the LBM using the direct forcing scheme with the immersed boundary method to simulate a deformable body in the flows. Xing and Nhan [15] applied the DLM/FD method to the LBM to simulate fluid-structure interaction such as a flexible filament in the wake of a cylinder.

<sup>†</sup> This paper was recommended for publication in revised form by Associate Editor Gihun Son

<sup>\*</sup> Corresponding author. Tel.: +82 2 2220 4452, Fax.: +82 2 2220 0445  
E-mail address: shlee@hanyang.ac.kr

Although there have been many developments in fluid-structure interaction solvers, there have been few for the finite element method (FEM) for the structure and the lattice Boltzmann method (LBM) for the fluid. The finite element method in structure solver has been widely used with great success as has the lattice Boltzmann method in fluid solver as well. We combined these two solvers for fluid-structure interaction problems. Among the many different boundary schemes of the lattice Boltzmann method, we used the immersed boundary treatment with a direct forcing scheme for the moving fluid-structure interface. We modified the immersed boundary treatment for the LBM to more accurately express flow and forces around the structures by introducing a coefficient reflecting the occupation ratio of the structure in the flow. For the flexible structure mechanics, we used the finite element method with a 2-dimensional element having 4 degrees of freedom at each node.

We applied the present scheme to the flow past a flexible plate in a free stream. This flow around a plate has been a classic example of bluff body flows. The formation of vortices at the sharp edges plays a major role in the flow pattern and induced force. Taneda and Honji [16] used the aluminum dust method to provide experimental visualizations of the flow around a flat plate. Dennis et al. [17] presented experimental and numerical results of flow around a plate normal to a free stream. They also presented results on the early time development of the wake and the effects of the blockage ratio. Dennis et al. numerically implemented a formulation in primitive variables that are not directly affected by the presence of the singularity. Koumoutsakos and Shiels [18] studied the flow around a zero thickness flat plate, impulsively started or uniformly accelerated normal to a free stream computationally. They used vortex element methods and showed the development of a number of centers of vorticity along the primary separating shear layer for the uniformly accelerated plate. The above results are for symmetric flows around a plate. In et al. [19] presented asymmetric results on the flow past a flat plate at various angles of incidence numerically for Reynolds numbers up to 30 using the vorticity-stream function form in body-fitted orthogonal coordinates. However, In et al. [19] only considered steady flow. The asymmetric unsteady flow around a plate normal to the free stream has often been observed in experimental and numerical results. This asymmetric unsteady flow can be characterized by the Strouhal number,  $St$ . Tamaddon-jahromi et al. [20] evaluated the flow for Reynolds numbers of 126, 250, and 500 using a Taylor-Galerkin/pressure-correction finite element algorithm, and compared the perturbed and unperturbed results. Najjar and Vanka [21] solved the flow around a flat plate normal to a free stream for Reynolds numbers of 100, 250, 500, and 1000 using a fractional step procedure with high-order spatial discretization. They studied vortex interactions such as vortex pairing, tearing and deformation in the near- and far-wake regions. These results have severe quantitative differences according to  $Re$ , but their trends are similar.

We compared the results of the present scheme with these

previous results on the flow around a rigid plate normal to free stream. In addition, we added the effects of the elasticity of a flat plate with asymmetric unsteady flow perturbed at the initial stage.

## 2. Fluid solver

### 2.1 The lattice Boltzmann method (LBM) with a single relaxation time

A popular kinetic model of LBM is the BGK model with a single relaxation time [22-24] as follows:

$$\frac{\partial f}{\partial t} + \xi \cdot \nabla f = -\frac{1}{\lambda} (f - f^{(0)}) \quad (1)$$

where  $f^{(0)}$  is the equilibrium distribution function (Maxwell-Boltzmann distribution function),  $f(x, \xi, t)$  is the particle velocity distribution function,  $x$  is the spatial position vector,  $\xi$  is the particle velocity vector,  $t$  is time, and  $\lambda$  is relaxation time. To solve the particle velocity distribution numerically, Eq. (1) is discretized by the discrete velocity set  $e_\alpha$ .

$$\frac{\partial f_\alpha}{\partial t} + \xi_\alpha \cdot \nabla f_\alpha = -\frac{1}{\lambda} (f_\alpha - f_\alpha^{(eq)}) \quad (2)$$

where  $f_\alpha(x, t)$  is a distribution function with the  $\alpha^{th}$  discrete velocity  $e_\alpha$  and  $f_\alpha^{(eq)}$  is the corresponding equilibrium distribution function in the discrete velocity space.

Eq. (2) is discretized in space and time as

$$\begin{aligned} f_\alpha(x_i + e_\alpha \delta t, t + \delta t) - f_\alpha(x_i, t) &= -\frac{1}{\tau} [f_\alpha(x_i, t) - f_\alpha^{(eq)}(x_i, t)] \\ f_\alpha(x_i + e_\alpha \delta t, t + \delta t) &= f_\alpha(x_i, t) + \Omega_\alpha(x_i, t), \end{aligned} \quad (3)$$

where  $\tau \left( = \frac{\lambda}{\delta t} \right)$  is the non-dimensionalized relaxation time,  $x_i$  is a position in the discretized physical space, and  $\Omega_\alpha \left( = -\frac{1}{\tau} (f_\alpha - f_\alpha^{(eq)}) \right)$  is the collision term. Eq. (3) can be solved with the following two steps.

#### 1) Collision Step

$$\tilde{f}_\alpha(x_i, t + \delta t) = f_\alpha(x_i, t) - \frac{1}{\tau} [f_\alpha(x_i, t) - f_\alpha^{(eq)}(x_i, t)] \quad (4)$$

#### 2) Streaming Step

$$f_\alpha(x_i + e_\alpha \delta t, t + \delta t) = \tilde{f}_\alpha(x_i, t + \delta t) \quad (5)$$

where  $\tilde{f}_\alpha$  is the post-collision state of the distribution function. These two steps are localized and simple to implement. A 9-velocity set model was used (D2Q9) as shown in Fig. 1. The equilibrium distributions for D2Q9 have form as follows:

$$f_\alpha^{(eq)} = \rho w_\alpha \left[ 1 + \frac{3}{c^2} (e_\alpha \cdot u) + \frac{9}{2c^4} (e_\alpha \cdot u)^2 - \frac{3}{2c^2} (u \cdot u) \right] \quad (6)$$

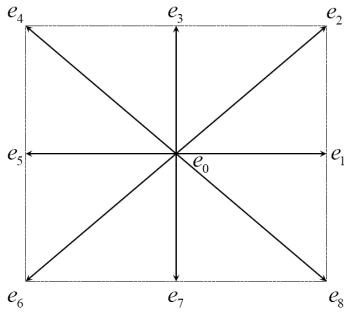


Fig. 1. D2Q9 lattice.

where  $e_\alpha$  is a discrete velocity set. The term  $e_\alpha$  is a 9-velocity set in D2Q9:  $e_\alpha = 0$  for  $\alpha = 0$ ,

$$e_\alpha = c \cos\left(\frac{(\alpha-1)\pi}{4}\right), c \sin\left(\frac{(\alpha-1)\pi}{4}\right) \text{ for } \alpha = 1, 3, 5, 7,$$

$$e_\alpha = \sqrt{2}c \cos\left(\frac{(\alpha-1)\pi}{4}\right), \sqrt{2}c \sin\left(\frac{(\alpha-1)\pi}{4}\right) \text{ for } \alpha = 2, 4, 6, 8,$$

where  $c = \left(\frac{\delta x}{\delta t}\right)$  is the lattice speed,  $\delta x$  is the lattice constant,  $\delta t$  is the time step, and  $w_\alpha$  is a weighting factor as follows:  $w_\alpha = 4/9$  for  $\alpha = 0$ ,  $w_\alpha = 1/9$  for  $\alpha = 1, 3, 5, 7$ , and  $w_\alpha = 1/36$  for  $\alpha = 2, 4, 6, 8$ .

In addition, there are diverse forms of the equilibrium distribution according to discrete velocity sets. The physical properties, such as density and momentum, are determined from the distribution function that is used as the primary variable in the LBM. The density is evaluated by  $\rho = \sum_\alpha f_\alpha = \sum_\alpha f_\alpha^{(eq)}$ , the specific momentum by  $\rho u = \sum_\alpha e_\alpha f_\alpha = \sum_\alpha e_\alpha f_\alpha^{(eq)}$ , the pressure

by  $p = \rho c_s^2 = \rho \frac{c^2}{3}$ , the viscosity by  $\nu = \left(\tau - \frac{1}{2}\right) c_s^2 \delta t$ , and

the speed of sound by  $c_s = \frac{c}{\sqrt{3}}$ .

### 2.2 The immersed boundary by the direct forcing scheme

We used the immersed boundary treatment for the no-slip boundary condition. The immersed boundary treatment adds the forcing term on the governing equations for the no-slip boundary condition. The forcing term can be related to the difference between the moving velocity of structure and the fluid velocity without structure on the boundary [25]. To determine the forcing term from velocity difference, the fluid momentum equation with forcing term can be written in the form [25]

$$\frac{\partial u}{\partial t} = \frac{u^{n+1} - u^n}{\Delta t} = -(u \cdot \nabla)u - \frac{\nabla p}{\rho} + \nu \nabla^2 u + f_f = rhs^{n+\frac{1}{2}} + f_f^{n+\frac{1}{2}} \quad (7)$$

where  $\rho$  is the density,  $p$  is the pressure,  $u$  is the velocity,

$rhs^{n+\frac{1}{2}}$  represents all usual flow forces, and  $f_f^{n+\frac{1}{2}}$  is the fluid-structure coupling forcing term. The above equation can be written for the additional force term as

$$f_f^{n+\frac{1}{2}} = \frac{u^{(d)} - u^n}{\Delta t} - rhs^{n+\frac{1}{2}} \quad (8)$$

where  $u^{(d)}$  is the desired velocity at the point where the force is applied. Eq. (8) is a principal characteristic of direct forcing methods. If there is no structure in the domain, the fluid-structure coupling force term  $f_f$  is ignored and the momentum equation can be written as

$$\frac{u^* - u^n}{\Delta t} = rhs^{n+\frac{1}{2}} \quad (9)$$

where  $u^*$  is the velocity without the structure boundary. If Eq. (8) is combined with Eq. (9), the modified forcing term can be written in the form

$$f_f^{n+\frac{1}{2}} = \frac{u^{(d)} - u^*}{\Delta t} \quad (10)$$

In general, the structure boundary does not coincide with the lattices used by the LBM, so interpolation is needed to obtain an adequate representation of the forcing interaction. Interpolation between the lattices of the LBM and the structure boundary can be written as

$$U(X_s) = \sum_f u(x_f) \delta_h(x_f - X_s) h^2 \quad (11)$$

$$f(x_f) = \sum_s F(X_s) \delta_h(x_f - X_s) \Delta s^2 \quad (12)$$

where  $x_f$  is a fluid lattice point with the uniform fluid lattice width  $h$  in all directions,  $X_s$  is a point distributed on the structure boundary with arc length  $\Delta s$ ,  $f_f (= f(x_f))$  is a distributed force by the structure to the flow at the fluid lattice point  $x_f$ ,  $F_s (= F(X_s))$  is a force at the structure boundary point  $X_s$ ,  $U(X_s)$  is the interpolated velocity at  $X_s$  from the fluid velocity  $u(x_f)$  of fluid lattice points  $x_f$ , and  $\delta_h$  is the regularized delta function proposed by Peskin [26].  $F_s$  is combined into the structure solver and adds some flexible deformation or rigid motion. From Eq. (10),  $F_s$  can be determined from the interpolated velocity on the structure boundary as

$$F_s^{n+\frac{1}{2}} = \frac{U^{(d)} - U^*}{\Delta t} \quad (13)$$

where  $U^{(d)}$  is the velocity of a point on structure boundary and  $U^*$  is the velocity without structure boundary.

When the force coefficient from  $F_s$  is evaluated, the participation ratio which is the ratio of fluid lattice points to effective interpolation lattice points is considered in order to predict a more accurate force coefficient:

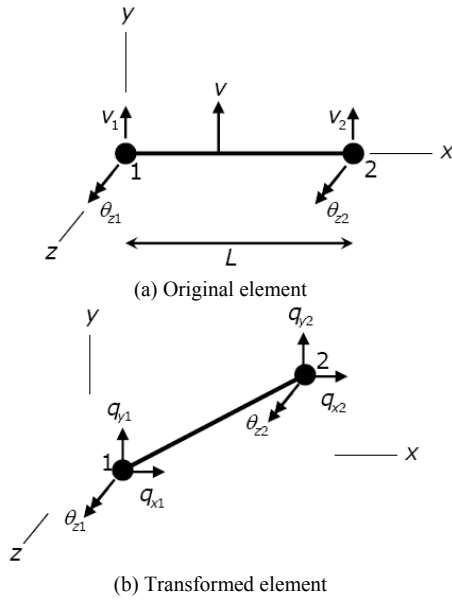


Fig. 2. One-dimensional bending element.

$$F'_s = F_s \frac{\text{Number of effective lattice points}}{\text{Number of fluid lattice points}} \quad (14)$$

$f_f$  can be combined into the LBM as a forcing term by

$$f_\alpha(x_i + e_\alpha \delta t, t + \delta t) - f_\alpha(x_i, t) = -\frac{1}{\tau} [f_\alpha(x_i, t) - f_\alpha^{(eq)}(x_i, t)] + \Delta t \frac{2w_i \rho}{c_s^2} e_\alpha \cdot f_f \quad (15)$$

The forcing term  $\Delta t \frac{2w_i \rho}{c_s^2} e_\alpha \cdot f_f$  is twice the forcing term used by other authors [15, 27]. The formulation of the forcing term in Eq. (15) is designed for a plate without thickness. A flat plate has a finite thickness and a solid area, but we used a plate without thickness. The zero thickness plate is thought of as the limit of two sides of a thick plate approaching each other. In this case, the solid area does not need to be considered, but the two sided boundaries of the plate must be considered. Therefore, the forcing term at the solid boundary should be the same as the forcing term in Eq. (15).

### 3. Structure solver

We used the finite element method for the flexible structure solver. The equations of the small, undamped motion for a generic point within a finite element can be written by using the principle of virtual work [28],

$$\int_V \delta \varepsilon^T \sigma dV = \int_V \delta u_d^T b(t) dV - \int_V \delta u_d^T \rho \ddot{u} dV \quad (16)$$

where  $\varepsilon$  is the strain vector,  $\sigma$  is the stress vector,  $q$  is the nodal displacement vector,  $u_d$  is the generic displacement vector,  $b(t)(= F_s(t))$  is the distributed body force vector, and

$\rho$  is the density of the structure. The generic displacement is related to the nodal displacement by  $u_d = Nq$ , where  $N$  is the shape function. The strain is related to the nodal displacement by  $\varepsilon = Bq$ , where  $B$  is the strain-displacement matrix. The stress and strain are related by  $\sigma = E\varepsilon$ , where  $E$  is elastic modulus. Eq. (16) can be organized with these relationships to form:

$$M\ddot{q} + Kq = p_b \quad (17)$$

where  $M = \int_V \rho N^T N dV$ ,  $K = \int_V B^T E B dV$ , and  $p_b = \int_V N^T F_s(t) dV$ . The inertia matrix  $M$  is composed of translational and rotational inertia. The translational inertia terms have greater value than the rotational term [28].

One-dimensional beam elements are used to represent bending. The vector of the nodal displacements becomes

$$q = \{q_1, q_2, q_3, q_4\} = \{v_1, \theta_{z1}, v_2, \theta_{z2}\} = \left\{ v_1, \frac{dv_1}{dx}, v_2, \frac{dv_2}{dx} \right\} \quad (18)$$

where  $v$  is the displacement normal to the element length, and  $\theta$  is the angle of small rotation. The description of an element is shown in Fig. 2. The bending element is composed of two nodes where each node has two degrees of freedom originally and is transformed along the global axes. The shape function is formed by Hermite polynomials.

### 4. Results

We validated the present scheme with four cases: the wake of a cylinder in a plane duct, the wake of a cylinder in free stream, oscillation of a flexible plate in a cavity, and the wake of a rigid plate. We applied the fluid-structure interaction solver to the flow around a flexible plate normal to a free stream to investigate the effect of flexibility on the wake. The flexible plate is fixed at the center.

#### 4.1 The flow around a cylinder in a plane duct at $Re=100$

We compared the results of the proposed boundary treatment to the well-known benchmark results of Schäfer and Turek [29]. The domain of the flow simulation is shown in Fig. 3.

The velocity distribution at the inlet is

$$U_x(0, y) = \frac{4U_m y(H-y)}{H^2}, \quad V(0, y) = 0, \quad (19)$$

where  $U_m = 1.5$  m/s,  $Re \left( = \frac{\bar{U}D}{\nu} = \frac{2U_m D}{3\nu} \right) = 100$ ,  $H$  the duct height,  $D$  the diameter of a cylinder and  $\nu$  the kinematic viscosity. At these conditions, the flow around the cylinder in the plane duct is unsteady, and the characteristics of the flow can be specified by the Strouhal number ( $St = f \frac{D}{2/3U_m}$ ).

When we used the LBM for this flow simulation, a moving wall type boundary condition was applied to the inlet of the plane

Table 1. Comparison of force coefficient and Strouhal number for the flow around a cylinder in a plane duct at  $Re = 100$ .

| Lattice Size |                        | (440,82) | (660,123) | (880,164) |
|--------------|------------------------|----------|-----------|-----------|
| $C_{D,max}$  | present                | 3.28     | 3.29      | 3.29      |
|              | Half-away bounce-back  | 4.56     | 3.52      | 3.20      |
|              | Schäfer and Turek [29] | 3.22     | ~         | 3.24      |
| $C_{L,max}$  | Present                | 1.03     | 1.04      | 1.04      |
|              | Half-away bounce-back  | 2.09     | 1.26      | 0.90      |
|              | Schäfer and Turek [29] | 0.99     | ~         | 1.01      |
| $St$         | Present                | 0.30     | 0.30      | 0.30      |
|              | Half-away bounce-back  | 0.28     | 0.29      | 0.29      |
|              | Schäfer and Turek [29] | 0.2950   | ~         | 0.3050    |

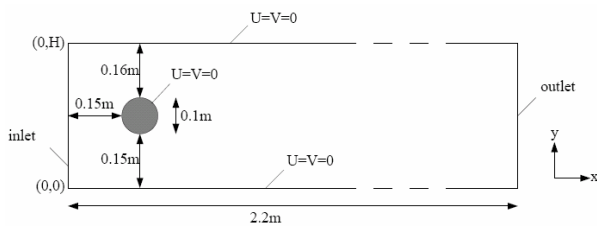


Fig. 3. The domain of flow simulation of unsteady flow around a cylinder in a plane duct.

duct [30], and the extrapolation scheme [31] was applied to the outlet.

Table 1. shows that the present simulation gave better accuracy than the half-away bounce-back boundary treatment that is the traditional boundary treatment in LBM. The present scheme using participation ratio compensated for the inaccurate force evaluation in the insufficient resolution around cylinder boundary. For lattice size (660,123), the value of  $C_D \left( = \frac{2F_x}{\rho \bar{U}^2 D} \right)$  using the present scheme had an error of less than 1.5%, and the value of  $C_L \left( = \frac{2F_y}{\rho \bar{U}^2 D} \right)$  had an error of less than 3.0%. Fig. 4 shows that the  $C_D$  and  $C_L$  using the present scheme agreed well with the reference. Our Strouhal number agreed with the value of Schäfer and Turek [29]. Fig. 5 shows the contours of the vorticity, streamwise velocity and pressure around a cylinder.

**4.2 The flow around a cylinder in free stream at  $Re=100$**

The Reynolds number is defined as  $Re = \frac{UD}{\nu}$ , where  $U$  is the free-stream velocity,  $D$  the diameter of a cylinder and  $\nu$  the kinematic viscosity. The shedding frequency is presented as the non-dimensional Strouhal number,  $St = f_s D / U$ , where  $f_s$  is the shedding frequency. The drag

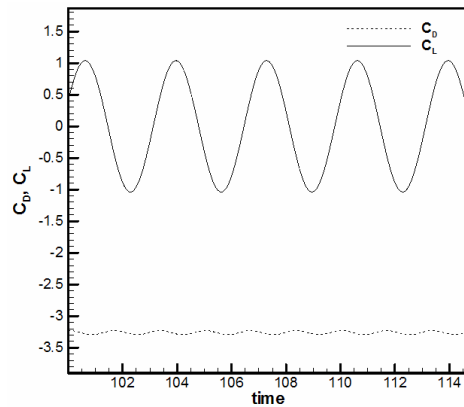


Fig. 4.  $C_D$ ,  $C_L$  of a cylinder in a plane duct according to time.

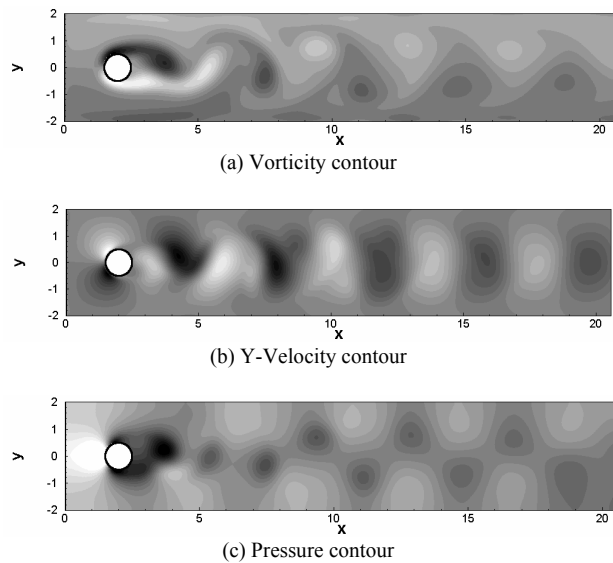


Fig. 5. Computed unsteady flow around a cylinder in a plane duct using the present scheme for  $Re = 100$ , lattice size (660x123).

and lift coefficients are defined as  $C_D = \frac{2F_x}{\rho U^2 D}$ , and  $C_L = \frac{2F_y}{\rho U^2 D}$ . The computational domain is  $28D \times 16D$  as

Fig. 6. A cylinder is placed  $8D$  from the inlet. This domain was used by Sharman et al. [33], and the lattice size of this domain is  $420 \times 240$ . The inlet boundary is implemented by a moving wall condition. The extended boundary scheme is used for infinite boundaries.

The computed drag and lift coefficients at  $Re = 100$  are shown in Fig. 7.

The computed vorticity contour and stream-lines are shown in Fig. 8.

The drag and lift coefficients and Strouhal number at  $Re = 100$  were compared with previous results of other researchers, shown in Table 2. The present simulation showed good agreement with the other results.

Table 2. Comparison of force coefficient and Strouhal number for the flow around a cylinder in free stream at  $Re = 100$ .

|             | Present | Park et al. [32] | Sharman et al. [33] | Kang [34] |
|-------------|---------|------------------|---------------------|-----------|
| $C_{D,max}$ | 1.33    | 1.33             | 1.33                | 1.33      |
| $C_{L,max}$ | 0.32    | 0.33             | 0.33                | 0.32      |
| $St$        | 0.162   | 0.165            | 0.165               | 0.165     |

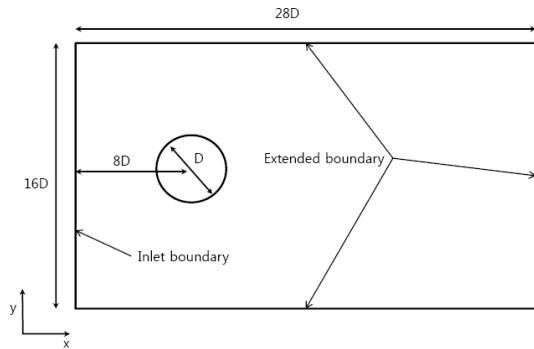


Fig. 6. The computational domain for the flow around a cylinder in free stream.

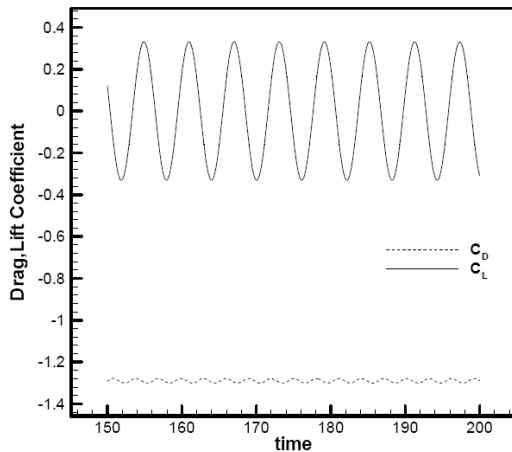
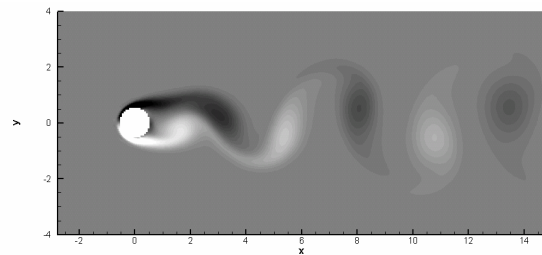


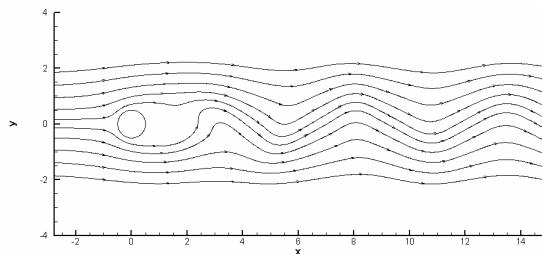
Fig. 7. Drag and lift coefficient of a cylinder in free stream at  $Re = 100$ .

**4.3 The oscillation of a flexible plate by initial perturbation in a cavity**

We validated the present code with the oscillation of a vertical flexible plate which was perturbed initially in a cavity. Fig. 9 shows the computational domain. The length, the thickness, and the width of the flexible plate are 1.0, 0.06, and 0.4 m, respectively. The plate has the following material properties: elastic modulus  $E = 2.5 \times 10^6 Pa$ , density of the plate  $\rho_s = 2550 kg/m^3$ , density of the fluid  $\rho_f = 1 kg/m^3$ , and three different dynamic viscosities of the fluid  $\mu = 0.2, 1.0, \text{ and } 5.0 kg/(m.s)$ . The plate was perturbed with a uniformly distributed load of 30 N/m initially until  $t \leq 0.5 s$ . Glück et al. [35] investigated the same problem by a three-dimensional simulation



(a) Vorticity contour



(b) Stream lines

Fig. 8. Vorticity contour and stream-lines of the flow around a cylinder in free stream at  $Re=100$ .

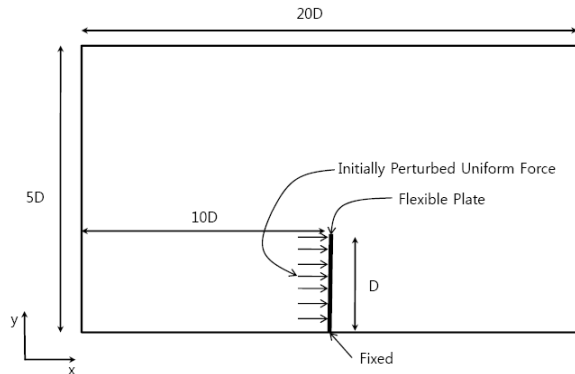


Fig. 9. The domain for a flexible plate oscillating in a cavity.

and Namkoong et al. [2] studied two dimensional case. We compared the results of present scheme with the results of Namkoong et al. [2] and Glück et al. [35] in Fig. 10. As for the previous other researchers' results, we showed only the peak points during each oscillation period in Fig. 10, which were enough to check the damping ratio and the frequencies of the oscillating displacement. The displacement of the free end of the flexible plate was damped faster, as the viscosity of fluid was higher. The damped displacement slopes and frequencies were well agreed with the previous researchers' results. The force of the flexible plate driven by fluid were shown in Fig. 11. The force was affected by the higher mode of the flexible plate which is also found in previous researchers' results [2, 35].

**4.4 The flow around a rigid plate at low Reynolds number**

Reynolds number is defined by  $Re = \frac{UD}{\nu}$ , where U is the free-stream velocity, D the length of a plate and  $\nu$  the

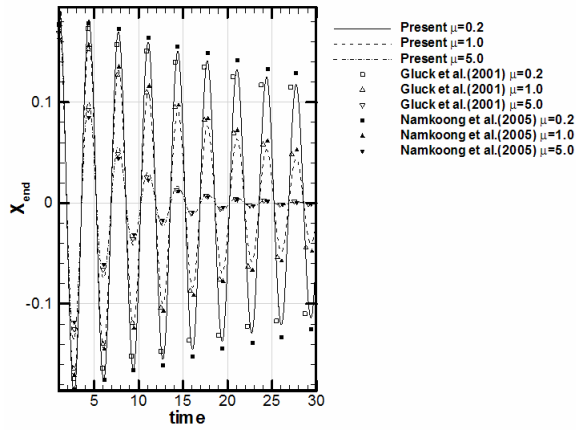


Fig. 10. The horizontal displacement of the free end of the flexible plate in a cavity.

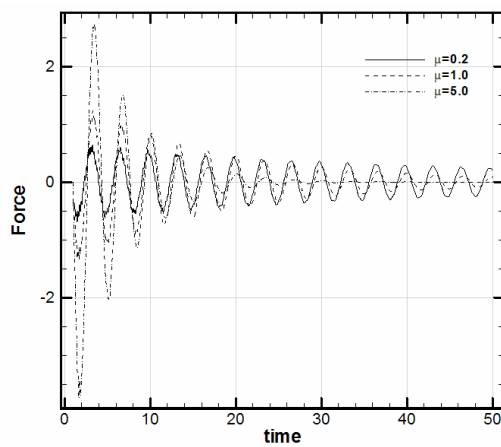


Fig. 11. The force of the flexible plate driven by fluid in a cavity.

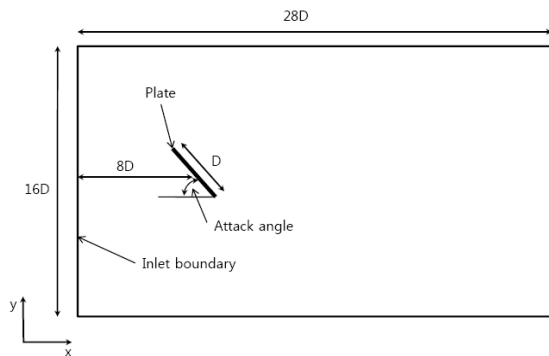


Fig. 12. The computational domain for the flow around a rigid & flexible plate.

kinematic viscosity. The computational domain is basically the same as the domain for the flow around a cylinder, and is shown in Fig. 12. The length of the wake and drag coefficient to  $Re$  for a plate normal to a free stream are compared with the well-known numerical and experimental results in Fig. 13. The present results agree well with these results.

To examine the accuracy of representing unsteadiness, wake length against time is plotted in Fig. 14. The present method

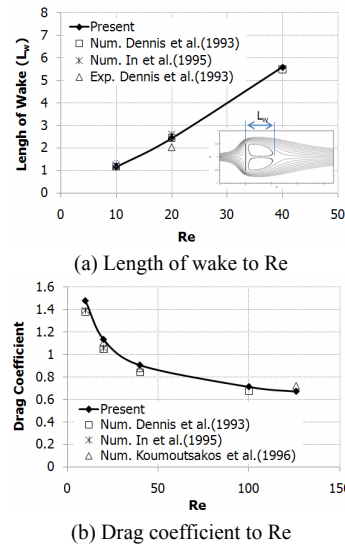


Fig. 13. The length of wake and drag coefficient according to  $Re$  for a plate normal to free stream.

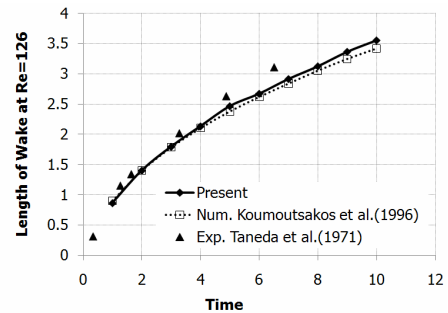


Fig. 14. The length of wake according to time for a plate normal to free stream.

shows good agreement with previous numerical and experimental results.

The flows over a plate inclined to a free stream were also compared with the previous results of In et al. [19]. The attack angle is defined as the angle between free stream and the plate. The streamlines of the inclined flat plate are shown in Fig. 15.

The force coefficients of the inclined plate are compared in Fig. 16. There is some deviation between our results and those of In et al. Our drag force is a little larger and our lift force was smaller than the values reported by In et al. [19]. In et al. used body fitted coordinates that can be more accurate to represent the force around sharp edge. But these discrepancies are small and the tendencies of the force coefficients according to the attack angle are quite similar.

#### 4.5 The flow around a flexible plate at a low Reynolds number

We placed a flexible plate normal to the free stream and fixed at the center. The analytic natural frequency of the plate with one end fixed is  $\frac{(1.875)^2}{2\pi} \sqrt{\frac{EI}{\rho AL^4}}$ , where  $L$  is the

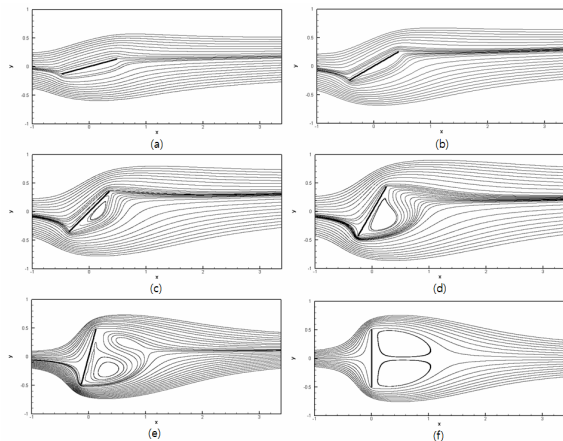


Fig. 15. Stream lines according to attack angle at  $Re = 10$  (a)  $15^\circ$ ; (b)  $30^\circ$ ; (c)  $45^\circ$ ; (d)  $60^\circ$ ; (e)  $75^\circ$ ; (f)  $90^\circ$ .

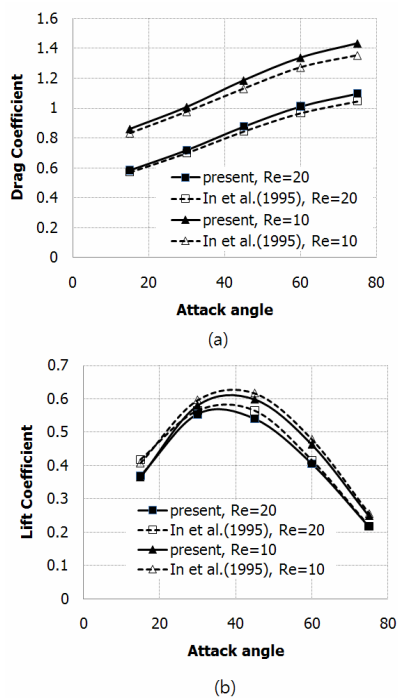


Fig. 16. Force coefficient according to attack angle (a)  $C_D$ ; (b)  $C_L$ .

length of plate,  $A(=BH)$  the area of the section of the plate,  $I(=BH^3/12)$  the moment of inertia, and  $E$  the elastic modulus. We set  $B$  to  $1m$  and  $H$  to  $0.02m$ . The  $L$  is  $0.5m$  because the center of the plate is fixed. We varied  $Re$ , whereas  $\rho$  was set to  $50,000kg/m^3$  and  $E$  to  $1 \times 10^7 Pa$ . This flexible plate has the analytic natural frequency of  $0.183$ . We introduced an initial perturbation to ensure unsteady flow. The perturbation was  $0.05 \cdot U \cdot \sin(\omega t)$  during the initial 100 steps.

The vorticity contours around the flexible plate according to  $Re$  are shown in Fig. 18 (compared to the cases of rigid plate in Fig. 17). The flow was steady at  $Re < 40$  in spite of the initial perturbation, which agrees with the critical  $Re$ . At  $Re = 40$ , weak vortices started to form far from the flexible plate. With

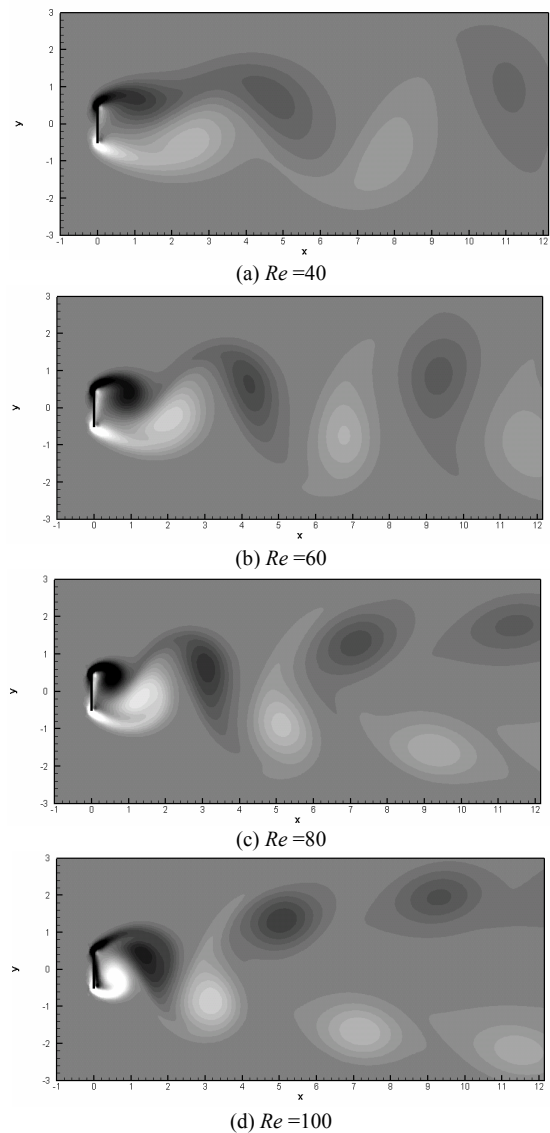


Fig. 17. Vorticity contour around a rigid plate according to  $Re$ .

increasing  $Re$ , stronger vortices were induced near the end of the flexible plate and the distances between vortices were shorter. Compared to the rigid plate, the width of the wake of the flexible plate was smaller because the deformed plate reduced the resistance to the flow.

The force coefficients and  $St$  are shown in Fig. 19. As shown in Fig. 20, the drag coefficients were characterized by two frequencies that were double the  $St$  based on the lift coefficient and the natural structure frequency of the flexible plate. The natural structure frequency component of the drag coefficient was a constant value at  $0.183$ . The magnitude of this frequency was also constant, whereas the magnitude of the frequency related to flow increased with increasing  $Re$  and was larger than the magnitude of natural frequency of flexible plate above  $Re = 100$ . The fact that the  $C_D$  has the natural frequency of the flexible plate means that the present scheme shows reasonable results. The natural structure frequency of the flexible

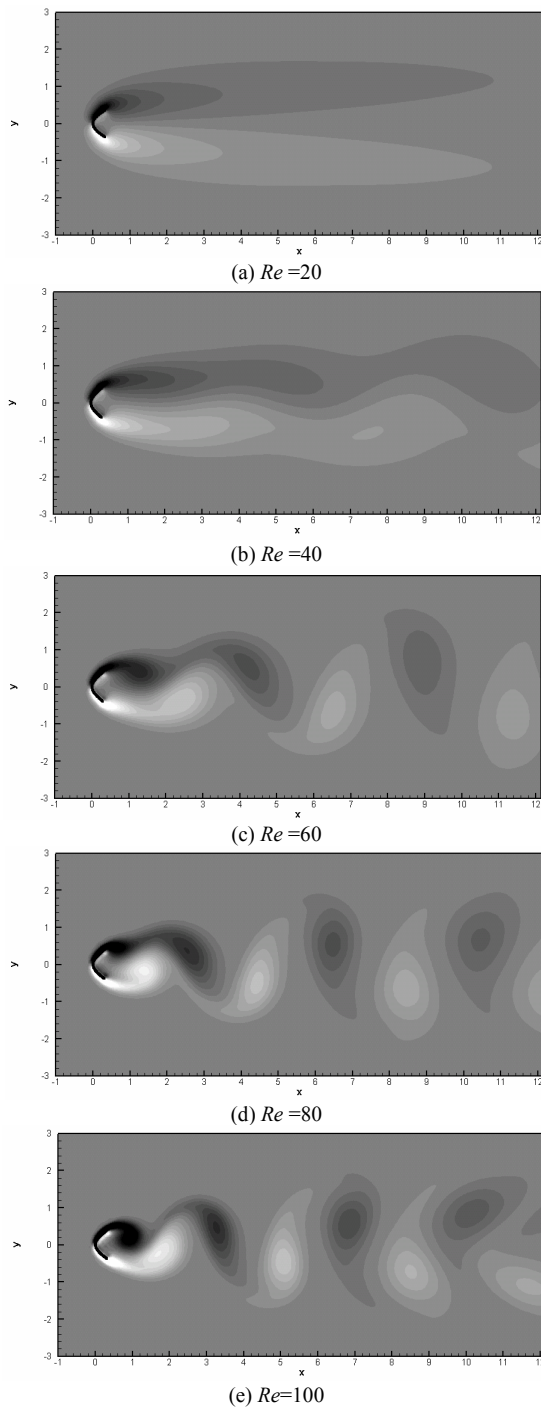


Fig. 18. Vorticity contour around a flexible plate according to  $Re$ .

plate decreased with increasing density exactly the same way as predicted theoretically, whereas the flow frequency was constant when the  $Re$  was kept constant.

The width of the wake decreased as the elasticity ( $E$ ) of the flexible plate decreased as in Fig. 21. This narrower wake was caused by increasing curvature. The flexibility of the flexible plate caused it to have a smaller force coefficient and resistance to the flow. The force coefficients according to elasticity ( $E$ ) are shown in Fig. 22. The  $St$  based on the lift coefficients of the

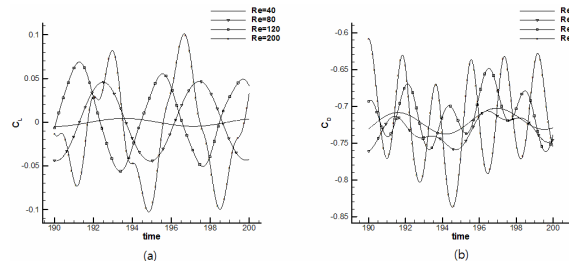


Fig. 19. Force coefficients (a) Lift coefficient of a flexible plate according to  $Re$ ; (b) Drag coefficient of plate according to  $Re$ .

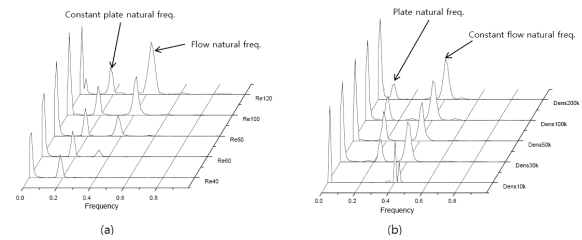


Fig. 20. Frequency domain of drag coefficients of a flexible plate (a)  $\rho = 5 \times 10^4$  according to  $Re$ ; (b)  $Re=100$ , according to  $\rho$ .

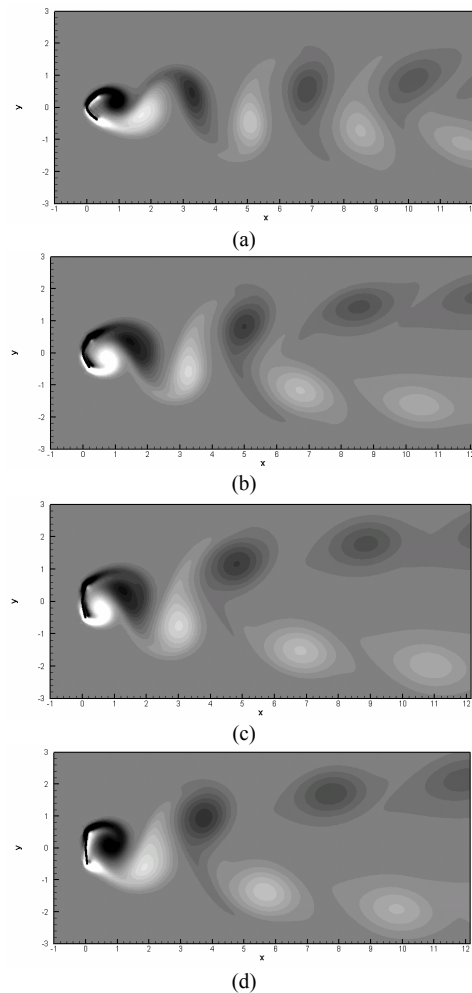


Fig. 21. Vorticity contour according to the elasticity of a flexible plate at  $Re=100$  (a)  $E = 1 \times 10^7$ ; (b)  $E = 2 \times 10^7$ ; (c)  $E = 5 \times 10^7$ ; (d)  $E = 1 \times 10^8$ .

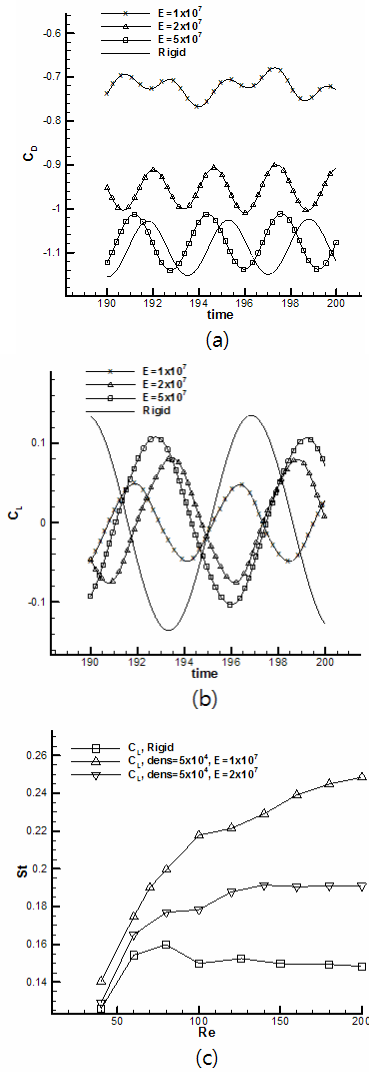


Fig. 22. Force coefficients and  $St$  of a flexible plate according to  $E$  (a) Drag coefficients; (b) Lift coefficients; (c)  $St$  based on  $Re$ .

plate was composed of three regions. When  $Re < 80$ ,  $St$  increased regardless of elasticity ( $E$ ).  $St$  in the  $Re > 120$  range differed according to the elasticity ( $E$ ) of the plate. In this region, the  $St$  of the rigid plate decreased with increasing  $Re$ , but the  $St$  of the flexible plate increased with increasing  $Re$ . In addition, the slope of the  $St$  curve of the flexible plate increased with smaller  $E$ . The rigid plate phenomenon of decreasing  $St$  with increasing  $Re$  when  $Re > 120$  has also been reported by Tamaddon-jahromi et al. [20] and Najjar and Vanka [21]. When  $80 < Re < 120$ , the dependence of  $Re$  and elasticity ( $E$ ) was not clear.

## 5. Conclusion

We have presented a method for the implementation of fluid-structure interaction using LBM for the fluid solver and FEM for the structure solver. The moving boundary problem was solved by a direct forcing scheme. We improved the direct forcing

scheme for application to very thin flexible plates. The applied scheme shows good agreement with previously known research results. We applied the present scheme to a flexible plate normal to a free stream flow as well. We were able to see that the elasticity had a role in the reduction of force coefficients of the flexible plate in a free stream flow, and found a change of  $St$  according to elasticity and  $Re$ . We found that the  $St$  of thin plates up to  $Re < 80$  increased regardless of flexibility, while the  $St$  in the range of  $Re > 120$  was dependent on the flexibility. When  $Re > 120$ , the  $St$  of very flexible plates increased with increasing  $Re$ , while the  $St$  of rigid plates decreased with increasing  $Re$ . In future work, we will estimate the locking phenomenon of a flapping plate using the developed scheme. Furthermore, we will develop a 3D scheme using LBM and FEM for the flapping of a flexible plate.

## Nomenclature

- $b(t)$  : Distributed body force vector,  $b(t) = F_s(t)$
- $B$  : Strain-displacement matrix of structure
- $c$  : Lattice speed,  $c = \frac{\delta x}{\delta t}$
- $c_s$  : Speed of sound
- $C_D$  : Drag coefficient
- $C_L$  : Lift coefficient
- $e_\alpha$  : Discrete velocity set
- $E$  : Elastic modulus of structure
- $f$  : Particle velocity distribution function
- $f_s$  : Shedding frequency
- $f_f$  : Distributed force by structure to flow at fluid lattice point  $x_f$
- $f_\alpha$  : Distribution function with the  $\alpha^{th}$  discrete velocity  $e_\alpha$
- $f_\alpha^{(eq)}$  : Equilibrium distribution function in the discrete velocity space
- $\tilde{f}_\alpha$  : Post-collision state of distribution function
- $f^{(0)}$  : Equilibrium distribution function
- $F_s$  : Force at structure boundary point  $X_s$
- $F_x$  : x-direction force component of structure
- $F_y$  : y-direction force component of structure
- $h$  : Uniform fluid lattice width
- $K$  : Stiffness matrix of structure
- $M$  : Inertia matrix of structure
- $N$  : Shape function for structure
- $p$  : Pressure
- $p_b$  : Equivalent external force vector to structure
- $q$  : Nodal displacement vector of structure
- $Re$  : Reynolds number
- $St$  : Strouhal number
- $t$  : Time
- $u$  : Velocity of flow
- $u_d$  : Generic displacement vector of structure
- $u^{(d)}$  : Desired velocity
- $u^*$  : Velocity without structure boundary
- $U$  : Velocity at structure boundary
- $v$  : Displacement normal to the element length of structure
- $w_\alpha$  : Weighting factor
- $x$  : Spatial position vector

|                 |  |
|-----------------|--|
| $x_f$           | : Point on fluid lattice point   |
| $x_i$           | : Position in the discretized physical space                             |
| $X_s$           | : Point on the structure boundary  |
| $\alpha$        | : Discrete velocity set index  |
| $\delta_h$      | : Regularized delta function   |
| $\delta t$      | : Time step  |
| $\delta x$      | : Fluid lattice constant   |
| $\Delta s$      | : Arc length of structure boundary between neighbored $X_s$              |
| $\varepsilon$   | : Strain vector of structure   |
| $\theta$        | : Angle of small rotation at structure node                              |
| $\lambda$       | : Relaxation time  |
| $\nu$           | : Viscosity of fluid   |
| $\xi$           | : Particle velocity vector   |
| $\rho$          | : Density of fluid   |
| $\rho_s$        | : Density of structure   |
| $\sigma$        | : Stress vector of structure   |
| $\tau$          | : Non-dimensionalized relaxation time, $\tau = \frac{\lambda}{\delta t}$ |
| $\Omega_\alpha$ | : Collision term   |

## References

- [1] H. Liu and K. Kawachi, A numerical study of undulatory swimming, *J. of Comp. Phys.*, 155 (1999) 223.
- [2] K. Namkoong, H. G. Choi, and J. Y. Yoo, Computation of dynamic fluid-structure interaction in two-dimensional laminar flows using combined formulation, *J. of Fluids and Structures*, 20 (2005) 51-69.
- [3] L. Bruno and D. Fransos, Evaluation of Reynolds number effects on flutter derivatives of a flat plate by means of a computational approach, *J. of Fluids and Structures*, 24 (2008) 1058-1076.
- [4] G. V. Papaioannou, D. K. P. Yue, M. S. Triantafyllou, and G. E. Karniadakis, On the effect of spacing on the vortex-induced vibrations of two tandem cylinders, *J. of Fluids and Structures*, 24 (2008) 833-854.
- [5] R. Glowinski, T. Pan, T. I. Hesla, and D.D. Joseph, A distributed Lagrange multiplier/fictitious domain method for particulate flows, *Int. J. Multiphase Flow*, 25 (1999) 755.
- [6] J. M. A. Stijnen, J. de Hart, P. H. M. Bovendeerd, and F. N. van de Vosse, Evaluation of a fictitious domain method for predicting dynamic response of mechanical heart valves, *J. of Fluids and Structures*, 19 (2004) 835-850.
- [7] Y. Liu, R. M. C. So, and Z. X. Cui, A finite cantilevered cylinder in a cross-flow, *J. of Fluids and Structures*, 20 (2005) 589-609.
- [8] M. Cheng, D.S. Whyte, and J. Lou, Numerical simulation of flow around a square cylinder in uniform-shear flow, *J. of Fluids and Structures*, 23 (2007) 207-226.
- [9] M. Bouzidi, M. Firdaouss, and P. Lallemand, Momentum transfer of a Boltzmann-lattice fluid with boundaries, *Phys. of Fluids*, 13 (2001) 3452-3459.
- [10] P. Lallemand and L. S. Luo, Lattice Boltzmann method for moving boundaries, *J. of Comp. Phys.*, 184 (2003) 406-421.
- [11] J. S. Lee and S. H. Lee, Boundary treatment for the lattice Boltzmann method using adaptive relaxation time, *Comp. and Fluids*, 39 (2010) 900-909.
- [12] Z. G. Feng and E. E. Michaelides, The immersed boundary-lattice Boltzmann method for solving fluid-particles interaction problems, *J. of Comp. Phys.*, 195 (2004) 602-628.
- [13] Z. G. Feng and E. E. Michaelides, A direct forcing method in the simulations of particulate flows, *J. of Comp. Phys.*, 202 (2005) 20-51.
- [14] Y. Sui, Y. T. Chew, P. Roy, and H. T. Low, A hybrid immersed-boundary and multi-block lattice Boltzmann method for simulating fluid and moving-boundaries interactions, *Int. J. Numer. Meth. Fluids*, 53 (2007) 1727-1754.
- [15] S. Xing and P. T. Nhan, Distributed Lagrange multiplier/fictitious domain method in the framework of lattice Boltzmann method for fluid-structure interactions, *J. of Comp. Phys.*, 206 (2005) 81-94.
- [16] S. Taneda and H. Honji, Unsteady flow past a flat plate normal to the direction of motion, *J. Phys. Soc. Japan*, 30 (1971) 262.
- [17] S. C. R. Dennis, W. Qiang, M. Coutanceau, and J. L. Launay, Viscous flow normal to a flat plate at moderate Reynolds numbers, *J. Fluid Mech.*, 248 (1993) 605-635.
- [18] P. Koumoutsakos and D. Shiels, Simulations of the viscous flow normal to an impulsively started and uniformly accelerated flat plate, *J. Fluid Mech.*, 328 (1996) 177-277.
- [19] K. M. In, D. H. Choi, and M. U. Kim, Two-dimensional viscous flow past a flat plate, *Fluid Dyn. Research*, 15 (1995) 13-24.
- [20] H. R. Tamaddon-Jahromi, P. Townsend, and M. F. Webster, Unsteady viscous flow past a flat plate orthogonal to the flow, *Comput. Fluids*, 23 (1994) 433-446.
- [21] F. M. Najjar and S. P. Vanka, Simulations of the unsteady separated flow past a normal flat plate, *Int. J. Numer. Methods Fluids*, 21 (1995) 525-547.
- [22] P. L. Bhatnagar, E. P. Gross, and M. Krook, A Model for Collision Processes in Gases. I. Small Amplitude Processes in Charged and Neutral One-Component Systems, *Phys. Review*, 94 (1954) 511.
- [23] S. Chen, H. Chen, D. Martinez, and W. Matthaeus, Lattice Boltzmann Model for Simulation of Magnetohydrodynamics, *Phys. Review Lett.*, 67 (1991) 3776.
- [24] Y. H. Qian, D. dHumières, and P. Lallemand, Lattice BGK models for Navier-Stokes equation, *Euro. Lett.*, 17 (1992) 479.
- [25] M. Uhlmann, An immersed boundary method with direct forcing for the simulation of particulate flows, *J. of Comp. Phys.*, 209 (2005) 448-476.
- [26] C. S. Peskin, The immersed boundary method, *Acta Numerica*, 11 (2002) 1-39.
- [27] A. Dupuis, P. Chatelain, and P. Koumoutsakos, An immersed boundary lattice-Boltzmann method for the simulation of the flow past an impulsively started cylinder, *J. of Comp. Phys.*, 227 (2008) 4486-4498.
- [28] W. Weaver, Finite Elements for Structural Analysis,

Prentice-Hall Inc. (1984).

- [29] M. Schäfer and S. Turek, Benchmark computations of laminar flow around a cylinder, Notes in Numerical Fluid Mechanics, (Vieweg Verlag, Braunschweig), 52 (1996) 547.
- [30] D. P. Ziegler, Boundary conditions for lattice Boltzmann simulations, *J. Stat. Phys.*, 71 (1993) 1171.
- [31] R. Mei, An Accurate Curved boundary treatment in the lattice boltzmann method, *J. of Comp. Phys.*, 155 (1999) 307.
- [32] J. Park, K. Kwon, and H. Choi, Numerical Solutions of Flow Past a Circular Cylinder at Reynolds Numbers up to 160, *KSME Int. J.*, 12 (1998) 1200-1205.
- [33] B. Sharman, F. S. Lien, L. Davidson, and C. Norberg, Numerical predictions of low Reynolds number flows over two tandem circular cylinders, *Int. J. Numer. Meth. Fluids*, 47 (2005) 423-447.
- [34] S. M. Kang, Characteristics of flow over two circular cylinders in a side-by-side arrangement at low Reynolds numbers, *Phys. Fluids*, 15 (2003) 2486-2498.
- [35] M. Glück, M. Breuer, F. Durst, A. Halfmann, and E. Rank, Computation of fluid-structure interaction on light weight

structures, *J. of Wind Eng. and Indust. Aerodyn.*, 89 (2001) 1351-1368.



**Ji Seok Lee** received his B.S. and M.S. in Mechanical Engineering from the Hanyang University, and currently is in the Ph.D program at Hanyang University. His research areas are in computational fluid dynamics and fluid-structure interactions.



**Sang Hwan Lee** received his B.S. degrees from Hanyang University, and the M.S. and Ph.D. from New York Buffalo State University. Prof. Lee is a Professor of the Department of Mechanical Engineering of Hanyang University. His research fields include parallel computing of fluid dynamics.